PTEP

Prog. Theor. Exp. Phys. **2015**, 00000 (18 pages)
DOI: 10.1093/ptep/0000000000

Measurement of the total muonium emission rate from silica aerogel using musr method (improved version showing the overall structure but some parts are still missing)

K. Ishida[1], K. Suzuki[2], T. Mibe[2], M. Iwasaki[3], J. H. Brewer[4], and S. Kamal[5]

[1]*RINE Nishina Center, RIKEN. Saitama 351-0198 ,Japan*
[*]*E-mail: ishida@riken.jp*
[2]*Institute of Particle and Nuclear Stueies (IPNS), High Energy Accelerator Research Organization (KEK), Ibaraki 305-0801, Japan*
[3]*Meson Science Laboratory, RIKEN, Saitama 351-0198, Japan*
[4]*Department of Physics and Astronomy, University of British Columbia, BC V6T 1Z1, Canada*
[5]*Laboratory of Advanced Spectroscopy and Imaging Research (LASIR), Department of Chemistry, University of British Columbia, BC V6T 1Z1, Canada*

A new method of measuring the muonium (Mu) emission from the silica aerogel to vacuum was developed using the muonium spin rotation. Here we measured the loss of the muonium spin polarization when the Mu in vacuum reached a metal foil placed near the Mu emission surface of the aerogel. The increase of the muonium spin relaxation rate under the presence of a metal foil was consistent with the rate expected for Mu reaching the metal. This method confirmed the total number of muoniums emitted including those staying near the surface, for which the previous measurement with the positron tracking method had been difficult.

Subject Index xxxx, xxx

1. Introduction

We are developing the slow muon beam production as a source of accelerated cold muon beam to be used for the muon g-2/EDM measurement planned at J-PARC [1]. Slow muons are produced in vacuum by ionizing thermal energy muoniums (Mu = μ^+e^-) emitted from materials surface. The choice of theproduction target is essential since the muonium emission efficiency largely depends on the materials. We observed at TRIUMF that the Mu emission rate from silica aerogel is enhanced by treating the aerogel surface with laser ablation [2–4]. High quality slow muon beam will be obtained by ionizing the muonium with intense Lyman-α laser.

In the measurements at TRIUMF, we measured the muon position distribution as a function of time after muon injection by tracking positrons from muon-decay using the muti-wire drift chamber. Although this is a poweful method to monitor the emission and drift of the Mu in vacuum, its slection of Mu in the near surface region suffered from background. Although

the detector itself had good spacial resolution, the track back resolution was limited to a few mm due mainly to the scatterig of the positrons at the foil separating the vacuum from the air. Since many muons stay in the sample and decay there, it was difficult to clearly separate the Mu in the vacuum region within 5 mm from the surface from such background.

Since thermal velocity of the muonium is of the order of 5 mm/μs, most of the emitted Mu stays in this region during the muon lifetime. In fact, previous measurement focused on region between 10 and 40 mm from the surafce. In principle, we can extrapolate the muonium yield data back closer to the surface with the help of a modeling. Previous measurements were compared with a model simulation combining muon stopping in the sample, muon diffusion in the sample, and muon drift in the vacuum with the initial velocity following Maxwell-Boltzman distribution. Even though all the data so far is consistent with the model, it is very much preferred if an independent confirmation is made.

We performed a new measurement using a completely different method, muon spin rotation (μSR) under an applied magnetic field ($\sim$0.22 mT). Muon spin rotation is a well known technique, which has been widely applied to studying material properties such as magnetism, supercondctivity and chemistry. Here, the muon beam is produced with the muon spin polarized and the muons are injected in a material under study. If we apply a magnetic field vertically to the initial munon spin direction, the muon spin precesses with a frequency of $\gamma_\mu = 0.13554$ MHz/mT. Some muon may form a muonium (Mu = μ^+e^-) though the formation probability largely depends on the material. Once Mu is formed, it precesses with a frequency of $\gamma_{Mu} = 14.0$ MHz/mT. In contrast, we will call the muons without forming Mu as diamagnetic muons. As the muon emits a positron preferentialy to the spin direction when it decays, development of the muon spin direction is monitored utilizing the asymmetric emisson of the muon decay positrons. Since the precession frequency is about 100 tmes different, it is easy to distinguish the Mu precession from that of a diamagnetic muon.

2. Principle of the method

We have shown that the muon, once stopped in silica aerogel, forms (65.5$\pm$1.8)% muoniums and (34.5$\mp$1.8)% diamagentic muons.[4]. The muonium precession relaxed only slowly (0.05 μs^{-1}) in the silica aerogel [2] under good vacuum environment. The relaxation rate increased almost linearly with the addition of oxygen into the sample environment. This indicates that nearly 100% on muonium are interacting with oxygen in the voids between the aerogel structure. It is considered that the muoniums leave the bulk material quickly and diffuse in the voids between the aerogel structure most of the muon lifetime. Some of the muoniums may have chance to reach the material free vacuum region and then drift freely in vacuum. We are interested in those emitted muoniums since we will be able to shoot a laser beam and the ionized muons can be extracted as low energy muons using electro-static field, as was demonstrated for the muoniums from hot tungsten [5].

It is expected that the muoniums make regular precession under a constant magnetic field applied vertically to its initial polarization. Mu precession is kept even after the muonium is emitted to vacuum. Here, if we put a metallic foil such as gold attached near to the aerogel surface, muoniums entering the metal are expected to become diamagnetic since it is known that no muonium is stable in a metal. Then the Mu precession will be disrupted as the precession frequency changes suddenly. This will be observed as the reduction of

the Mu precession amplitude with the time after muon beam injection. For example, if 10% of the formed muonium has reached the foil by a given time, the precession amplitude should decrease to 90%. Thus, the precession spectrum gives us information on the timing distribution of the muoniums reaching the foil.

(note: We may add here an equation for the precession with frequency change.)

Fig. 1 Schematic of the Mu precession damping by metal foil. (note: A schematic figure showing the principle is planned here.):

3. Experimental method

The measurement was carried out at the RIKEN-RAL Muon Facility in ISIS, RAL [6]. We set an aerogel sample with a gold foil stacked near the surface on the downstream side relative to the beam direction. The schematic figure of the target arrangement is shown in Fig. 2. The sample was set in a vacuum chamber in the ARGUS μSR spectrometer at RIKEN-RAL. The same aerogel as used in the TRIUMF S1249 measurement in 2017 [4] was used. The aerogel sample was synthesized[7] at Chiba University and the laser ablation was performed in UBC. Parameters of aerogel samples used in the measurement are summarized in Table 1. Each sample had an area of 50 mm x 50 mm and was 8.8 mm thick. The aerogel density was 23.2 mg cm^{-3}. The muonium emission probability measured at TRIUMF is also shown in the table. The probability is defined as the number of muon decays in vacuum between 10 to 40 mm from the sample surafce divided by the number of decays from all the region. The detailed description of the target and the result of the TRIUMF measurement is reported elsewhere[4].

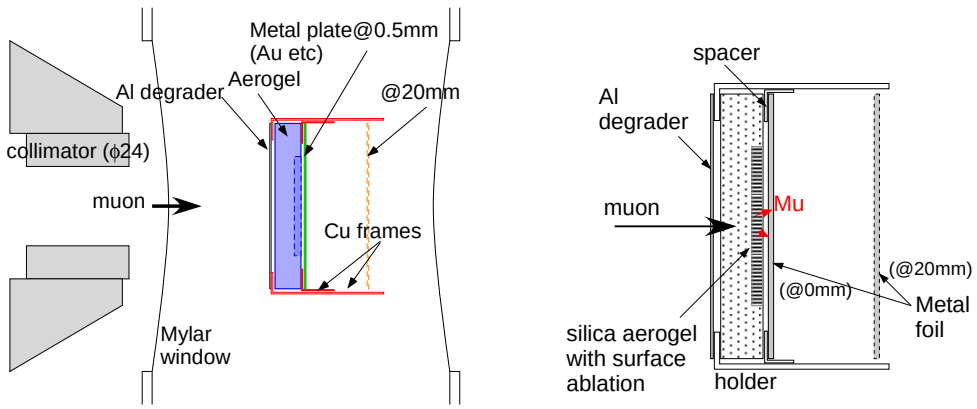

Fig. 2 Schematic of the target arrangement. (Left) The muon beam passed the aluminum degrader before entering the silica aerogel sample. By changing the muon momentum, the stopping positions of the muons were controlled. (Right) The distance from the aerogel surface to the metal plate can be changed by changing the spacer. The minimum distance was 0.3 mm.

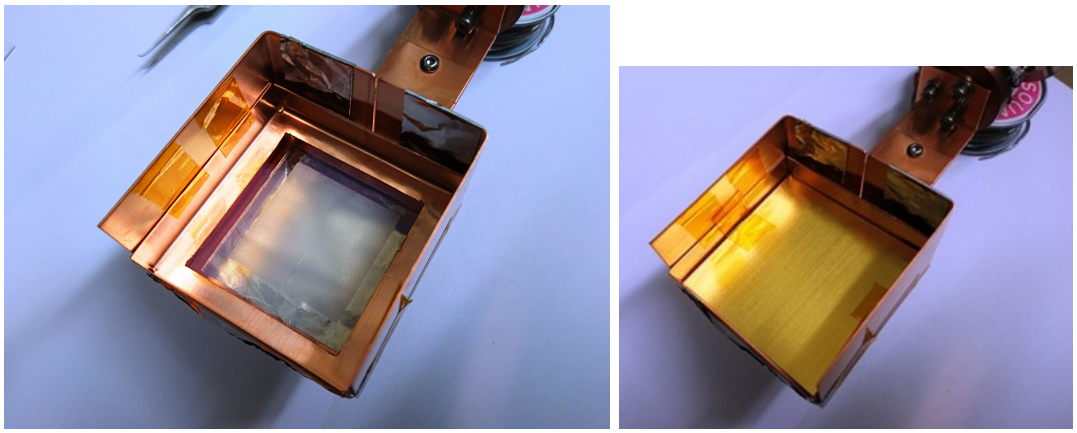

Fig. 3 Left: Photo of the target assembly when a silica aerogel (#18) was set in the holder. The ablated square region can be seen clearly. Right: Same with the gold plate covering the sample.

Target S18 had the best emission rate among tested and target S9 had slightly less emission. Target S8 was without ablation and the emission rate was 10 times smaller. Since sample S18 and S9 had the laser ablation in the region 30 mm x 30 mm at the center, the muon beam was collimated by a lead collimator with 24 mm innner diameter at 6 cm upstream the sample. Simulaiton indicates that more than 95 % of the muons stopping in the aerogel are within the ablated region of 30 mm x 30 mm. (note: We may remove this paragraph and Table 1 if S8 and S9 data are not shown.)

Table 1 Silica aerogels used as the target. All had an area of 50 mm × 50 mm and 8.8 mm thickness with 23.2 mg/cm^3 density.

Target ID	Ablation area [mm x mm]	Hole diameter and pitch [mm]	Hole depth [mm]	Mu emission per stop (S1249 2017)
S18	30 x 30	0.165, 0.25	1.0	0.0276(2)
S9	30 x 30	0.1, 0.15	1.25	0.0218 (2)
S8	no			0.00292 (6)

The list of the metal plates used for stopping Mu are shown in Table 2. All were purchased from Nilaco and were kept sealed until they were mounted for the measurement. The foil thickness was chosen so that it is thick enough to stop all the muons that have passed through the aerogel even at the highest momentum selected. After the aerogel and the metal foil were assembled in the holder they were set in a vacuum chamber and the chamber was evacuated. We waited until the vacuum level was below 10^{-2} Pa before starting μSR measurement as we know that the oxygen can depolarize the muonium. The measurement for silica powder with added oxygen has shown k = (2.55+-0.13) x 10^{-10} cm^3 molecule^{-1} s^{-1} [8] and a similar dependence was observed for silica aerogel also[2]. Assuming a similar rate constant for silica aerogel, the depolarization by air at 10^{-2} Pa is expected be 0.00014 μs^{-1} and is negligibly small.

Table 2 Metals used as the muonium quencher.

Material (purity)	Size	Thickness	
	[mmxmm]	[mm]	[g/cm^2]
Gold	50 x 50	0.10	0.193
Silver	50 x 50	0.20	0.211
Copper	50 x 50	0.30	0.269
Nickel	50 x 50	0.20	0.178
Aluminum	50 x 50	1.0	0.270
Graphite	50 x 50	2.0	0.450

The experimental setup is schematically shown in Fig. 2. The muon beam passed the beamline exit window, air gap and the mylar window of the vacuum chamber before entering the target assembly. The target assembly consisted of an aluminum degrader, aerogel target and a metal foil. These were housed in a frame made of pure copper sheets with thickness either 0.3 or 0.5 mm. Photo of the target assembly is shown in Fig. 3. The aerogel was set so that the ablated surface is at the downstream side. The aluminum degrader thickness was set as 100 μm so that the muons pass a similar amount of materials as that for our previous measurements at TRIUMF before entering the silica aerogel. By varying the muon beam momentum, the muons can be either stopped in the aluminum degrader, in the aerogel or in the metal foil downstream. We were especially interested in two conditions. One is when the muons stopping distribution is peaked at the center of the aerogel, which we will call "full-stop" as most of the muons stop in the aerogel only. The other is where the muon's stopping depth distribution peaks at the downstream edge of the aerogel, which we will call "half-stop" as the muon is expected to stop in the aergel and the downstream metal by half and half. For the metal set in the downstream, we mainly focused on the gold foil as its surface condition is expected to be free from oxidization. Even though, other metals were also tested to see if there is any difference. In addition to the choice of different metals, we also had choice on the distance between the aerogel surface and the metal foil. In the default setting with the minimum spacing, the metal sheet was set after 0.3 mm thick frame structure to avoid direct contact of the metal to the ablated surface. The holder frame and the spacer both had 40 mm x 40 mm opening so that they do not interfere the muon injection and the muonium coming out. Additional spacers (10 mm or 20 mm) were added when we vary the distance between the aerogel surface and the metal foil.

The measurement was performed at ARGUS in the Port 2 of the RIKEN-RAL beam line at ISIS, Rutherford Appleton Laboratory.[6]. The muon beam momentum is selectable and, for each setting, the momentum spread is approximated by a Gaussian with about 2 % in standard deviation (4.6 % in FWHM). At the central momentum of 21.5 MeV/c, this corresponds to 10 mg/cm^2 range in silica and the aerogel sample (20 mg/cm^2) is thick enough to cover 95 % of the stopping distribution.

The analysis was done on the asymmetry spectra, which was defined as $P(t) = (F - \alpha B)/(F + \alpha B)$, where F(t) is the muon dcay positron events observed by the upstream detector, B(t) is that for the downstream detector and α is the correction factor to cancel the difference in detector efficiencies, which was determined separatly using precession under

magnetic field of 2.0 mT. We fitted the asymmetry spectra with the following equation, where each term is for muonium precession, diamagnetic muon precession, and the baseline. (note: We may prefer to set α=1 as the choice of the momentum affects α and make the comparison difficult.)

$$P(t) = A_D \cos(\omega_D t + \phi_D) \exp(-\lambda_{Mu} t) + A_{\mathrm{Mu}} \cos(\omega_{\mathrm{Mu}} t + \phi_{\mathrm{Mu}}) \exp(-\lambda_{Mu} t) + A \qquad (1)$$

The Mu precession amplitude (A_{Mu}) was determined from the measurement under 0.22 mT transverse magnetic field and that of diamagentic muon (A_D) under 2.0 mT so that a reliable fit can be made by using several precession periods in the time window of typically 10 μs. In the case of 2.0 mT, We dropped the muonium precession term from the fit since the precession of the Mu was too small to be observed due to the large dephasing caused by the muons arriving at diffrent timing in the beam bunch width (70 ns) longer than the Mu precession period (36 ns), In the case of the 0.22 mT, the diamagnetic muons made less than one precession in the observation time range. Nevertheless, the diamagnetic precession was included in the fit with the frequency fixed to that expected to correctly analyse to long time muSR spectrum. Clear changes of the precession spectra were observed as shown in Fig. 4 by changing the momentum as 20, 20.5, 21.5 , 22.7 and 25 MeV/c.

4. Result

4.1. Selection of muon momentum

Considering that the diffusion length is much smaller than the muon stopping distribution width, optimum condition for Mu emission is achieved by selecting the beam momentum so the muon's stopping distribution peaks at the surface of the aerogel.

Fig. 5 shows the fitted precession amplitude of the diamagnetic muons and that of the muoniums. Here, twice the Mu precession amplitude (2 A_{Mu}) is plotted to better reflect the formation fraction considering that half the polarization is lost when the muon forms a muonium. In addition, we divided the observed amplitude by a correction factor of 0.76 for muonium and 0.95 for diamagentic muons in order to compensate the amplitude reduction caused by the dephasing caused by different injection timing of the muons within the finite pulse beam width (70 ns FWHM). The muonium precession amplitude peaked at 21.5 MeV/c and became nearly zero at both ends where the muons either stopped in the aluminum degrader or in the gold metal at downstream. The sum of the precession amplitudes ($A_{tot} = 2A_{Mu} + A_{\mu}$) was almost independent of the muon momentum, even though the materials of muon stopping is different. This clearly indicates that there is no missing fraction in the silica aerogel. At 21.5 MeV/c, the muonium formation fraction ($2A_{Mu}/A_{tot}$) is calculated as 58.8±1.0%. Considering about 5±2% of the muons may stop in metals at this condition, the corrected Mu fraction in silica aerogel is 61.9±1.3%, which is in agreement with our previous measured value 65.5±1.8%.

The Mu amplitude becomes about half of the maximum at 22.7 MeV/c, so we selected this momentum as the half-stop condition. Other momenta of interest are 21.5 MeV/c ("full stop" in aerogel), 24 MeV/c (full stop in gold foil), 20.5 MeV/c (half stop in aerogel and aluminum degrader), 20.0 MeV/c (full stop in aluminum degrader). We mainly focus on 22.7 MeV/c and 21.5 MeV/c and call them as "half-stop" and "full-stop" condition, respectively.

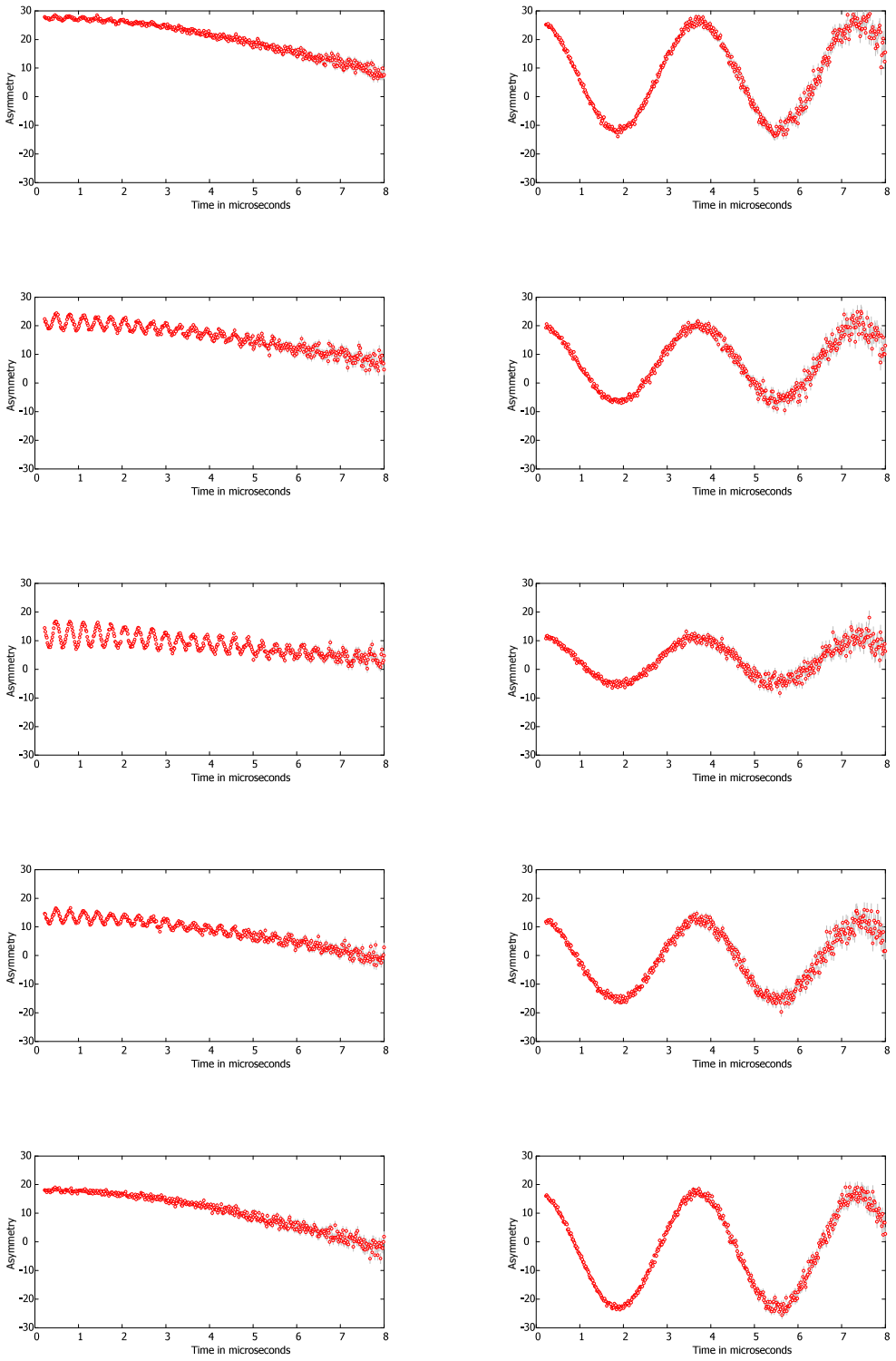

Fig. 4 μSR asymmetry spectrum as the momentum was varied as 20, 20.5, 21.5, 22.7 and 24 MeV/c (top to bottom). Each was measured under the applied field of 0.22 mT (left) and 2.0 mT (right). The correction factor α was fixed as 1 to show how the baseline changes with the momentum.

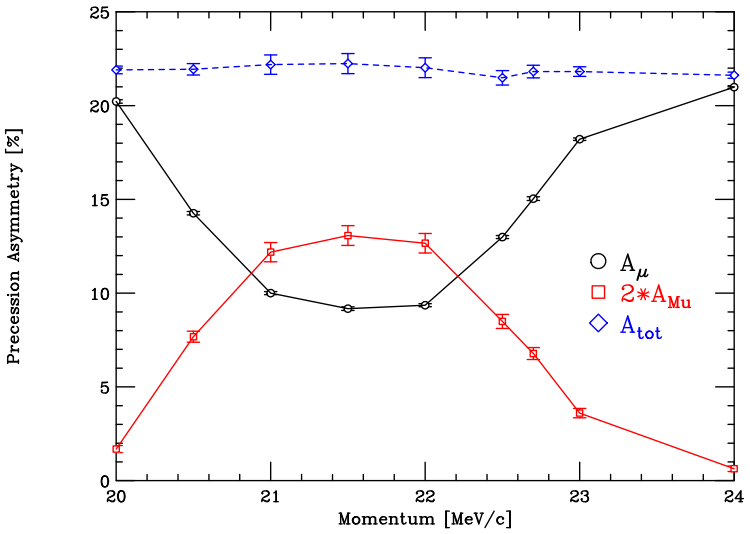

Fig. 5 Momentum dependence of the measured muoniumprecession amplitude ($2 \times A_{Mu}$ and the diamagnetc muon precession amplitude (A_D). The amplitude of the Mu precession was doubled to compensate for the loss of polarization while forming the muonium. Each was measured under applied field of 0.22 mT and 2.0 mT, respectively. the sum is shown to verify there is no significant missing fraction.

A simulation of muon stopping depth distribution under the assumption of Gaussian momentum distribution is shown for the above momentum settings in Fig. 6. It well reproduces the change of muonium fraction with momentum.

4.2. Run-by-run result by changing the sample condition

The run-by-run relaxation rates as the quenching metal or the muon stopping condition (full-stop and half-stop) were varied are shown in Fig. 7. Full data measurement took about 36 hours and each data point took about 40 minutes. It can be seen that there is clear difference between the rate at '"full-stop" and '"half-stop" conditions. Detailed analysis is given in the following sections.

4.3. Muonium precession in full-stop condition

Since there are Mu relaxations even in the full-stop condition, we need to know this background relaxation precisely. For all the target arrangement, we measured both full-stop and half-stop condition. The fluctuation of the relaxation rate in "full-stop" condition was not much beyond the statistical error. To study the cause of the relaxation, we added all the data and examined the relaxation function. The fit to the sum data as shown in Fig. 8 gave the relaxation rate $(0.0391 \pm 0.0014)\ \mu s^{-1}$.

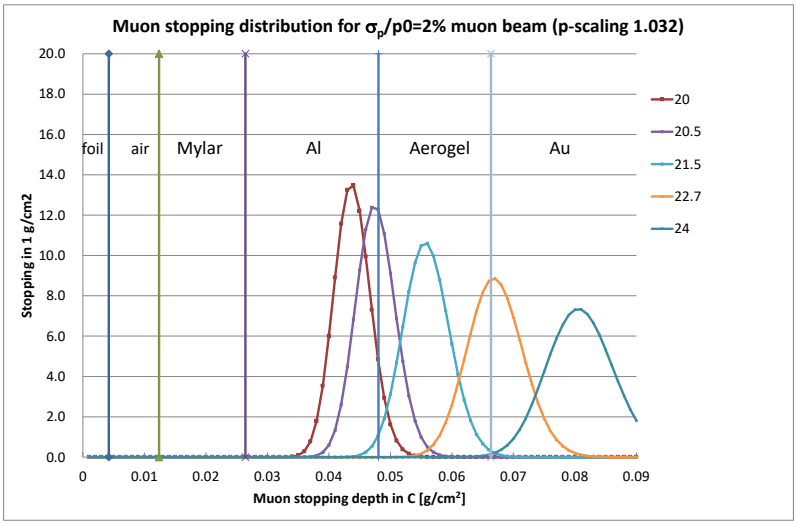

Fig. 6 Simulated muon stopping distribution in silica aerogel and other materials. Momentum distribution with of 2% (FWHM 4.7%) is assumed. Thickness of each material is normalized to that of the carbon considering the slight material dependence of the muon stopping power.

(note: This part would need clearer description or may be removed.) There are several possible contributions to the relaxation. The relaxation may occur in the material at the very early stage. There may be interaction with oxygen, which should be small under good vacuum condition. The Mu may stay some time at the surface of the structure, which is known to be small because if the short duration at room temperature. There might be also relaxation due to field inhomogeneity or the field fluctuation with time. The first one only appears as a loss near time zero and the effect seems small. Only the last one makes gaussian relaxation while others tend to give exponential relaxation.

4.4. Muonium precession in half-stop condition and extraction of the Mu quenching rate

Figure 9 shows the spectrum for all the half-stop runs with the gold foil set at 0.3 mm distance. The fitted Mu relaxation rate was (... μs^{-1}) and was significantly larger than that in full-stop condition. Similar increase was observed for all other metals used. Table 3 shows the fitted Mu relaxation rate for all the sample conditions. All the data with the foil at the minimum distance show similar rates exept that for nickel. The rate with the gold at 10 mm or 20 mm shows smaller effect reflecting the additional time needed for the emitted Mu to reach the foil. The relaxation for the nickel (at RUN 69085) had exceptionally high relaxation reflecting the strong disturbance on the magnetic field by the nickel magnetization and the data was not used in the further analysis.

The full-stopn and half-stop data are more clearly seen by extracting the Mu precession part only. The slow diamagnetic muon precession part was removed from the spectra using

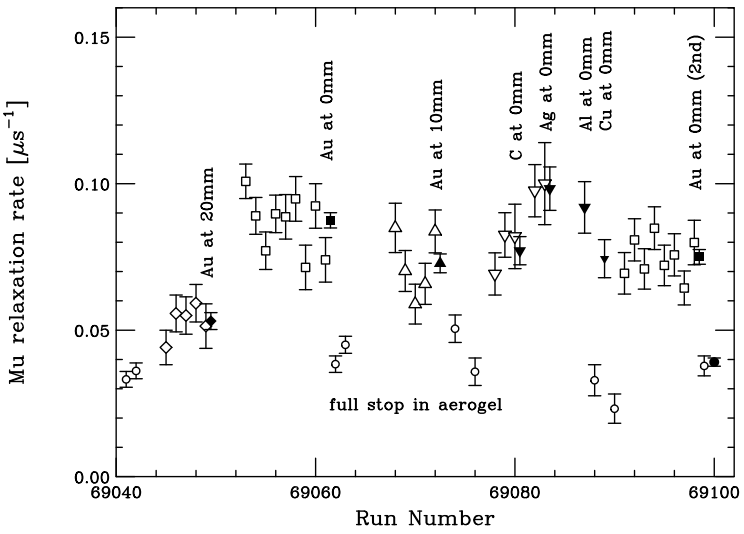

Fig. 7 Run-by-run change of the relaxation rate as a sequence of the run number. Sample conditions are shown in the figure. Full stop conditions runs are shown with circle symbols while half stop condition runs use other symbols. The filled symbols show the average for runs preceeding the symbol under the same condition. Detailed descriptions of the sample conditions are given in the text. The nickel data is above the range and is not plotted here.

the fitted values. $P_{Mu}(t) = P(t) - A_D \cos(\omega_{\rm D} t + \phi_{\rm D}) \exp(-\lambda_D t) + A_{Base}$. The result in Fig. 10 shows a simple precession around the zero line. The vertical axis of the half-stop data was doubled to compensate the smaller stopping fraction in half-stop condition. It is clearly seen that the Mu relaxation for the half-stop case was significantly larger than that in full-stop condition.

As a rough estimation, if the muon escape the aerogel with rate λ_v, the relaxation rate will increase by λ_v. The result of Table 3 indicates that about 4 % of the muonium escape the aerogel per μs. Since the escape may not be given by a simple exponential, we will make more detailed discussion in the next subsection.

4.5. Detailed analysis - precession envelope plot

The relaxation can be more clearly seen by showing the data using Mu precession envelope. Using the Mu precession data as seen in Fig. 10, the precession amplitude was calculated for each precession period of 320 ns using $P^{env}_{Mu}(j) = \Sigma P_{Mu}(t_i) \cos(\omega_{\rm Mu}(t_i) + \phi_{\rm Mu}) / \cos^2(\omega_{\rm Mu} t_i + \phi_{\rm Mu})$ where the sum is over 20 data points each with 16 ns bin. Comparizon for the full stop case and the half-stop case with the gold plate at 0.3 mm are shown in Fig. 11. Although we lose the time resolution with this method (as each point has 320 ns), the plot shows the difference in the long time relaxation behavior very clearly.

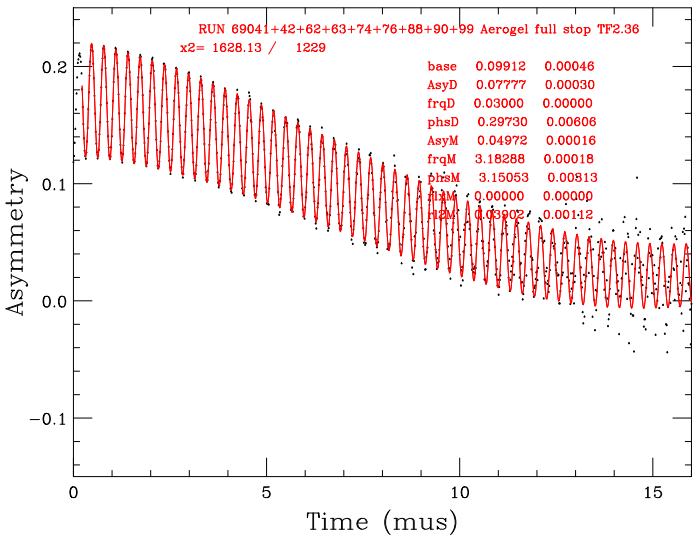

Fig. 8 Sum of MuSR spectrum under 0.223 mT with muons stopping in the center of silica aerogel (21.5 MeV/c).

Table 3 Fitted Mu relaxation rate .for variiuos conditions.

Material	relaxation rate $[\mu s^{-1}]$
Full Stop(all)	0.0391 (14)
Gold(1st)	0.0875 (26)
Gold(2nd)	0.0750 (25)
Gold(10mm)	0.0728 (32)
Gold(20mm)	0.0531 (29)
Silver	0.0983 (74)
Copper	0.0744 (65)
Nickel	0.234 (28)
Aluminum	0.0919 (88)
Carbon	0.0771 (48)

The relaxation includes both contributions from the intrinsic relaxation in the silica aerogel and also contribution form the Mu reaching the metal. We extracted the Mu quenching contribution by dividing the data with $\exp(-\lambda_{Mu}0)$. The plot is shown for the data with Au at 0.3, 10, and 20 mm distance in Fig. 12.

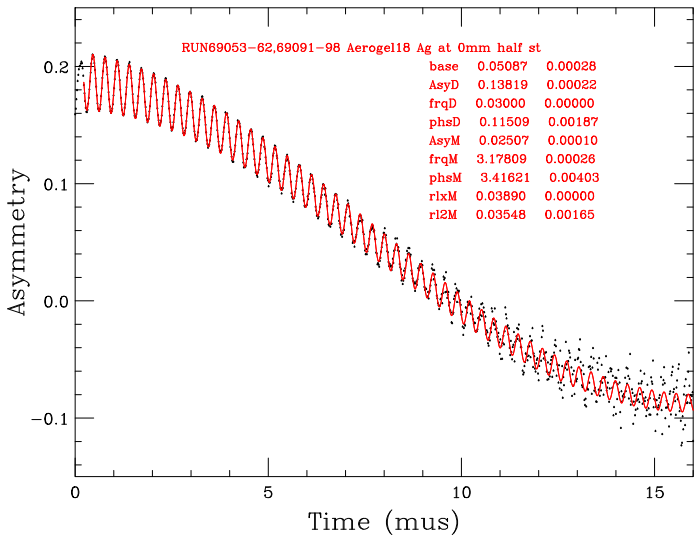

Fig. 9 MuSR spectrum under 0.223 mT with muons stopping near the rear edge of silica aerogel (22.7 MeV/c) with a gold foil placed at 0.3 mm.

4.6. Detailed analysis of the relaxation function - simple diffusion model

(note: This subsection is far from complete.) So far we simply utilized exponential relaxation for the fitting of the relaxation. Actually, the arrival time might show different distribution from exponential

We consider the spread of Mu formed at distance x_0 from the surface. Using a simple diffusion model with effective diffusion constant D, its distribution after time t can be expressed by a Gaussian $G(x, x0) = (1/\sqrt{2\pi}\sigma_D)\exp(-(x+x_0)^2/2\sigma_D^2)$ where $\sigma_D = \sqrt{Dt}$. In the case with boundary where no Mu can return, the probability of Mu having left the boundary at $x = 0$ is $P_{out}(t, x_0) = 2\int_0^\infty G(x, x_0)dx$, where the factor 2 reflects the boundary condition at x=0 that allows the Mu to pass in one way only. The stoppig distribution at half-stop condition can be approximated by a Gaussian with peak at the surface edge, $G_{stop}(x_0) = (1/\sqrt{\pi}\sigma_R)\exp(-x_0^2/2\sigma_R^2)$ where $-x_{thick} < -x_0 < 0$. The fraction of the Mu outside the aerogel after time t is

$$\begin{aligned} P_{out}(t) &= \int_{-x_{thick}}^{0} G_{stop}(x_0)P_{rem}(t, x_0)dx_0 \\ &= \int_{-x_{thick}}^{0} dx_0(1/\sqrt{\pi}\sigma_R)\exp(-x_0^2/2\sigma_R^2)\int_0^\infty dx(1/\sqrt{2\pi}\sigma_D)\exp(-(x+x_0)^2/2\sigma_D^2) \end{aligned} \quad (2)$$

In the case where the diffusion length σ_D is much smaller than the stoppping distribution σ_R, we can set $\exp(-x_0^2/2\sigma_R^2) \sim 1$. The total emission by time t is propoortional to $t^{1/2}$. (note: The derivation should be shown.) This is understandable as those muons that are in the diffusion distance can contribute to emission and that increases with $t^{1/2}$. Thus, Mu remaining in the aerogel is proportional to $1 - at^{1/2}$, where a is a factor related to the muon

stopping fraction per length. Usually, the second term is small (which means that most of the muons remain in the aerogel), so this can be approximated as exp(-$at^{-1/2}$), which is a well known square-root exponential relaxation function. We may generalize the relaxation function as $exp(-at^{-\beta})$, which is now the stretched exponential relaxation. Using this fitting function with β as a free parameter, we can judge which model well describes the relaxation.

If we use the gaussian distribution of the stopping distribution with peak at the edge of the silica aerogel, we cannot get analytical form and should rely on numerical integration.

4.7. Effect of distance to the foil

(note: This subsection is far from complete.) Here we compare the data with different gold distance. One clear feature is the shift of the baseline, which is well understood as the solid angle for the positrons from the muon decay chanegs as the gold plate position was shifted. The reduction of the relaxation as seen in Table 3 as the metal foil was moved away by x_g from the aerogel surface is a strong evidence that the effect is caused by the Mu emitted in vacuum.

Here we estimate the effect quantitatively. The relaxation was extracted in a similar method as above and the fit result is shown using the precession ebvelope in Fig. 12.

Actually, the relaxation function is even more complicated because the arrival time to the gold foil is also dependent on the drift velocity in vacuum, whose distribution is expected to follow Maxwell-Boltzman distribution and is also emission angle dependent. Under the simplest assumption replacing the velocity by a single average velocity, this actullay works as the delayed start of the relaxation, $P_{gap}(t) = P(t + t_{drift})$, where $t_{drift} = x_g/v$.

5. Conclusion and Future Prospects

We carried out the first determination of the total muonium emission rate using the μSR method. The result was consistent with the rate from our previous measurement using the positron tracking method assuming the diffusion model. One advantage of the present measurement is that it can be performed using the standard μSR setups that are available at most muon facilities and does not require the sophisticated tracking detectors. So this method can be used for quick evaluation of Mu emission from various aerogel samples.

We would like to note that this method can be used to measure the surfac interecation of the muonium as the quenching would affect the relacxation. rate So far the effect looks almost independent of the material as far as we use metals or graphite. We are interested in testing other materials such as insulators or organic materials.

Acknowledgment

We thank Dr. Tabata and Prof. H. Kawai for their sipport to produce silica aerogel samples. We thank Dr. G. Marshall and Dr. A. Olin for the discussion on the Mu diffusion model and the Mu surface interaction

References

[1] M. Abe et al.: Prog. Theor. Exp. Phys. (2019) C01.
[2] P. Bakule et al.: Prog. Theor. Exp. Phys. (2013) 103C01.
[3] G. A. Beer et al.: Prog. Theor. Exp. Phys. (2014) 091C01.
[4] J. Beare et al.: to appear Prog. Theor. Exp. Phys. (2020).
[5] P. Bakule et al.: Nucl. Instrum. Methods Phys. Res., Sect B **266**, 335 (2008).

[6] T. Matsuzaki et al.; Nucl. Instrum. Meth. in Phys. Res. A **465**, 365 (2001).
[7] M. Tabata et al.: Nucl. Instrum. Methods Phys. Res., Sect A **668**, 64 (2012).
[8] G.M. Marshall et al.; Phys. Lett. **A 65**, 351 (1978).

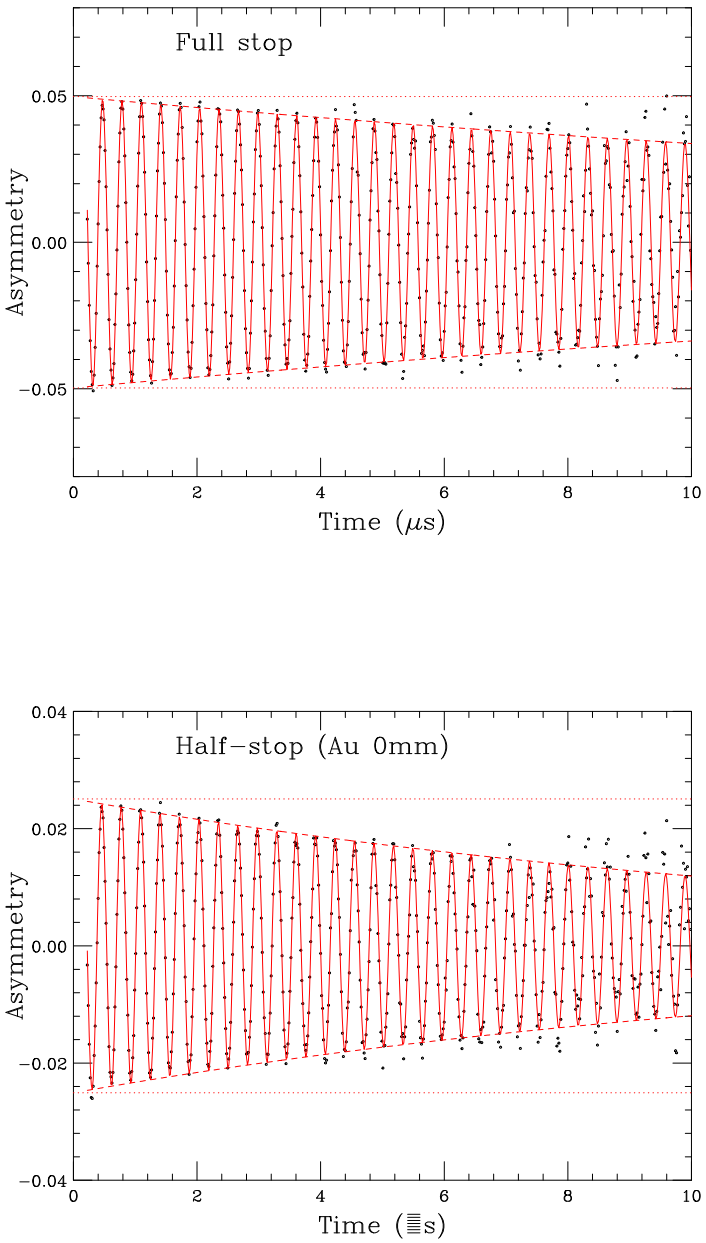

Fig. 10 Comparison of the Mu relaxation in full-stop and half-stop conditions. Only the Mu perecession is shown by subtracting the diamagnetic muon precession using the fitted result. Note the difference in the vertical scale reflecting the different stopping fraction in the silica aerogel.

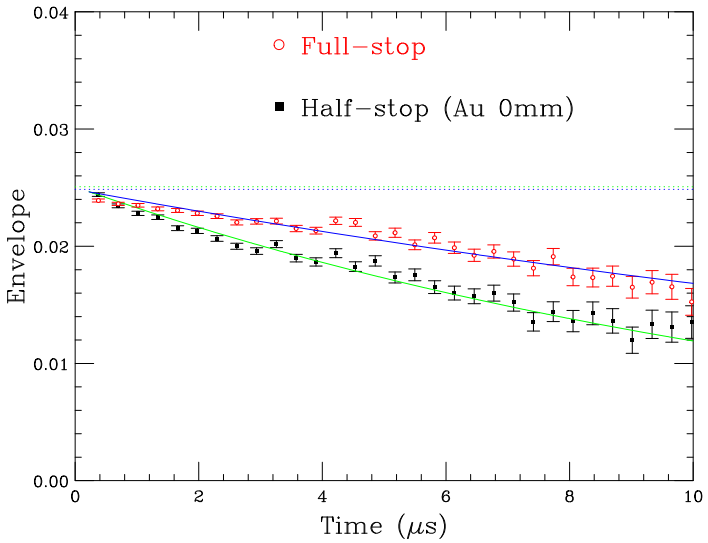

Fig. 11 Mu precession envelope spectra in the full-stop condition and the half-stop condition with Au at 0.3 mm. . The solid line is a result of fit with the exponential relaxation fuction. The data for the full-stop is divided by 2 in order to compensate for the dufferent stopping fraction.

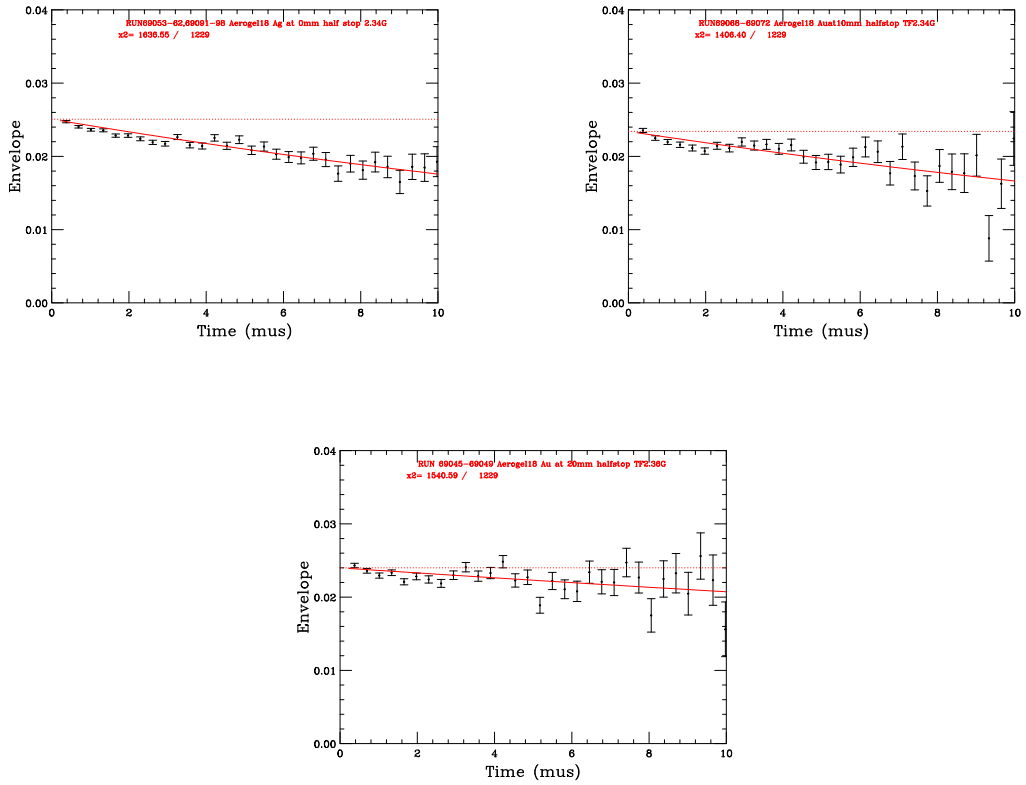

Fig. 12 Mu precession envelope spectra for the case with gold foil at 0.3 mm, 10 mm and 20 mm. The data was divided by the exponential decay due to the intrisic Mu relaxation so as to show the Mu quenching effect only.

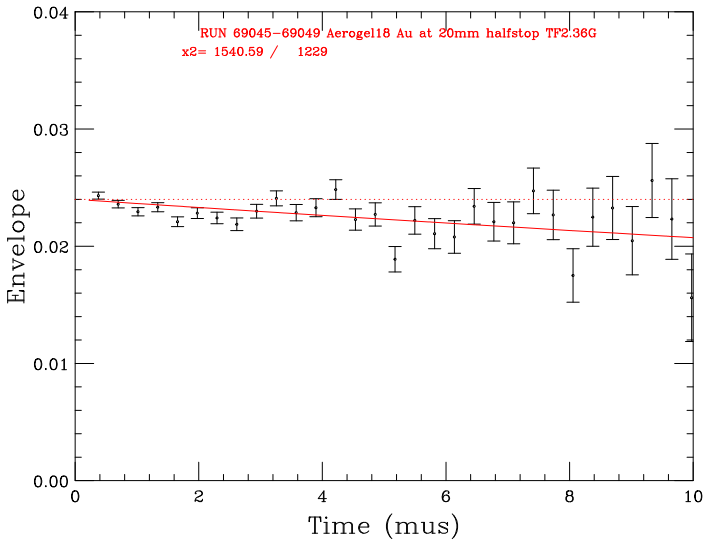

Fig. 13 The fit of the relaxation function in two ways (note: fits are not done yet), one including the delay time and the other without. The delay time was set as 3 μs considering the thermal velocity $v = 7mm/\mu s$ and the distance $x_g = 20mm$.